Medical Image Analysis 69 (2021) 101946

Contents lists available at ScienceDirect

Medical Image Analysis

journal homepage: www.elsevier.com/locate/media

Evaluation of a novel navigation platform for laparoscopic liver surgery with organ deformation compensation using injected fiducials

Egidijus Pelanis[a,b,1,*], Andrea Teatini[a,c,1], Benjamin Eigl[d], Alois Regensburger[e], Amilcar Alzaga[e], Rahul Prasanna Kumar[a], Tobias Rudolph[d], Davit L. Aghayan[a,b,i], Carina Riediger[f], Niclas Kvarnström[g], Ole Jakob Elle[a,c], Bjørn Edwin[a,b,h]

[a] The Intervention Centre, Oslo University Hospital Rikshospitalet 0424, Oslo, Norway
[b] Institute of Clinical Medicine, University of Oslo 1072, Oslo, Norway
[c] Department of Informatics, University of Oslo 1072, Oslo, Norway
[d] Cascination AG 3008 Bern, Switzerland
[e] Siemens Healthineers 91301 Forchheim, Germany
[f] University Hospital Carl Gustav Carus, Technische Universität Dresden, 01307 Dresden, Germany
[g] Sahlgrenska University Hospital, 41345 Goteborg, Sweden
[h] Department of Hepato-Pancreatic-Biliary surgery 0424, Oslo University Hospital, Oslo, Norway
[i] Department of Surgery N1, Yerevan State Medical University, 0025 Yerevan, Armenia

ARTICLE INFO

Article history:
Received 26 May 2020
Revised 28 November 2020
Accepted 15 December 2020
Available online 29 December 2020

Keywords:
Image guided surgery
Augmented reality
Target registration error
Laparoscopic liver resection
Intraoperative imaging
Navigation

ABSTRACT

In laparoscopic liver resection, surgeons conventionally rely on anatomical landmarks detected through a laparoscope, preoperative volumetric images and laparoscopic ultrasound to compensate for the challenges of minimally invasive access. Image guidance using optical tracking and registration procedures is a promising tool, although often undermined by its inaccuracy. This study evaluates a novel surgical navigation solution that can compensate for liver deformations using an accurate and effective registration method. The proposed solution relies on a robotic C-arm to perform registration to preoperative CT/MRI image data and allows for intraoperative updates during resection using fluoroscopic images. Navigation is offered both as a 3D liver model with real-time instrument visualization, as well as an augmented reality overlay on the laparoscope camera view. Testing was conducted through a pre-clinical trial which included four porcine models. Accuracy of the navigation system was measured through two evaluation methods: liver surface fiducials reprojection and a comparison between planned and navigated resection margins. Target Registration Error with the fiducials evaluation shows that the accuracy in the vicinity of the lesion was 3.78±1.89 mm. Resection margin evaluations resulted in an overall median accuracy of 4.44 mm with a maximum error of 9.75 mm over the four subjects. The presented solution is accurate enough to be potentially clinically beneficial for surgical guidance in laparoscopic liver surgery.

1. Introduction

The laparoscopic approach for liver surgery has become more widely accepted within the growing list of procedures Hilal et al. (2018) with patients reporting higher quality of life after laparoscopic compared to open liver resections Fretland et al. (2019). For colorectal metastasis (CRM), parenchyma-sparing liver resections focus on removal of lesions while preserving as much healthy liver tissue as possible, with only the sufficient margins around the lesions. These procedures can be relatively simple for small lesions located superficially. However, complex procedures, such as posterior-superior segments, require extensive planning of the resection to ensure removal of vascular territory with pathology and still maintaining safe resection margin Aghayan et al. (2018).

To prepare for complicated surgical approaches, surgical planning and diagnostics are ordinarily conducted through medical imaging such as Computed Tomography (CT) and Magnetic Resonance Imaging (MRI). Through segmentation processes, these images can be used to create patient-specific 3D models that can support decision-making Berardi et al. (2019) and improve spatial understanding Pelanis et al. (2019). Furthermore, with addi-

* Corresponding author.
E-mail address: egidijus@pelanis.eu (E. Pelanis).
[1] Denotes equal contributions.

https://doi.org/10.1016/j.media.2020.101946

tional software tools, these models can be used for resection planning Palomar et al. (2017) FDA (2013) Soler et al. (2015).

To follow the surgical plan, during laparoscopic liver surgery, surgeons conventionally rely on visualised anatomical landmarks detected through the laparoscope camera or the laparoscopic ultrasound. These structures are used by the surgeon to correlate, in their mind, the prepared surgical plan with the intraoperative space. This approach may lead to inaccuracies, especially if the landmarks used to perform this correlation are difficult to visualise and couple with confidence. Hence, to bridge the gap between planning and surgery, as well as to aid the surgeon in conducting a safe and accurate procedure, surgical navigation solutions are being tested clinically Ntourakis et al. (2016) Hallet et al. (2015) and emerging in the market Thompson et al. (2018) Prevost et al. (2019).

Surgical navigation devices aim to provide additional information to enhance both lesion localization and visualization of vascular territories. For example, using superimposed virtual segmented volumes onto the physical perspective, known as Augmented Reality (AR), or as 3D interactive models Modrzejewski et al. (2019) Thompson et al. (2015) Teber et al. (2009) Thompson et al. (2018) Nicolau et al. (2009) Soler et al. (2014) Quero et al. (2019) Bernhardt et al. (2017). Surgical navigation is achieved through a combination of instrument tracking and registration processes, which often require input from the surgeons. Previous studies show that user dependency Thompson et al. (2018) Teatini et al. (2019), instrument tracking error Teatini et al. (2018), registration inaccuracy Thompson et al. (2018) Teatini et al. (2020) and liver deformation Zachariadis et al. (2020) are often the causes of inaccuracy in navigation systems. The extent of inaccuracy varies due to different setups, algorithms and organ of interest, although, for laparoscopic liver navigation, overall inaccuracies, reported in the literature, ranging from 8.7 to 42 mm Teatini et al. (2019) Thompson et al. (2018) Modrzejewski et al. (2019) Luo et al. (2020). Approached utilizing intraoperative CBCT/fluoroscopy and stereo laparoscopic images for registration have been researched and tested although without a TRE measurment during in vivo investigation Mountney et al. (2014). The aim of this study is to assess a novel navigation solution for liver laparoscopy which requires a simple, yet accurate, registration procedure, with a less user-dependent update possibility which can work even in the occurrence of large soft tissue deformations.

2. Materials and methods

Approved by the National Animal Experimentation Board [project ID: 12633] and in accordance with Norwegian regulations concerning the use of animals in experiments [FOR-2015-06-18-761], a pre-clinical trial was conducted on four porcine models from 2019 to 2020 to evaluate the presented navigation system. This to ensure a realistic conditions of laparoscopic liver resection with the assistance of a surgical navigation system and have results transferable to clinical use.

The proposed surgical navigation system relies on percutaneously injected gold tracking fiducials Kothary et al. (2009) around the lesion. These tracking fiducials have been used in clinical use during radiotherapy treatment, and are certified medical devices which can be injected before the surgery. The fiducials are used to perform registration tasks between volumetric images or registration updates using fluoroscopic images throughout the resection procedure, which allows the system to compensate for organ deformations. A schematic of the workflow for this solution is depicted in Fig. 1. Surgical navigation is achieved through a series of rigid transformations, utilizing optical instrument tracking applied to both the laparoscope camera and the surgical instruments. The proposed solution for surgical navigation offers guidance both as an interactive 3D liver model with real-time instrument visualization, as well as through a 3D AR overlay on the laparoscopic camera view (an example is shown in Fig. 4).

The navigation solution was tested in a state-of-the-art hybrid Operation Room (OR), which allows acquisition of contrast-enhanced CT (through a sliding gantry CT), Cone Beam CT (CBCT) and fluoroscopic images (using a robotically controlled C-arm), in a single OR, directly while the subject is on the surgical table. Evaluation of the navigation system was conducted through the assessment of Target Registration Error (TRE), computed using both laparoscopically inserted fiducials on the liver surface Teatini et al. (2019), as well as a comparison between the planned and marked resection margin on the liver surface following the navigation guidance.

2.1. Experimental protocol

The navigation solution was tested within a hybrid OR, equipped with a Siemens Healthineers GmbH ® SOMATOM CT scanner and an ARTIS pheno C-arm, which were used to acquire medical images directly on the operating table. An Aesculap ®E-insteinvision 30° oblique stereo laparoscope camera was used for laparoscopic video acquisition. Surgical navigation was visualized using a research version of the CAS-One AR system by CAScination AG ®. The system is based on CAScinations ® CAS-One AR product (CE Class 1 release in July 2017) and extends its functionality by a prototype software displaying AR overlays on laparoscopic images based on data received from a software provided by Siemens Healthineers. Tracking of the laparoscope camera and surgical instruments were performed through optical tracking with a Northen Digital Incorporated ®Polaris Vicra. The OR was prepared with conventional equipment for laparoscopic liver resection with the addition of an ultrasound machine for percutaneous needle placement to inject the gold fiducials used for registration.

2.1.1. Dataset description

A pre-clinical trial was conducted using a total of four porcine models, with weights ranging from 45 to 61kg. The dataset includes tracked stereo-video recordings using a calibrated laparoscopic camera, pre- and intraoperative contrast-enhanced CT and fluoroscopic acquisitions, as well as instrument tracking and registration transformation matrices. Every acquired transformation matrix has a global origin in P (following the diagram in Fig. 5), which is an optical markerplate which indicates the position of the patient, rigidly connected to the surgical table. Timestamps in the recordings were used to compute the duration of the steps presented in the workflow (Fig. 1) and described in Section 2.2.3.

2.1.2. Injection of artificial lesion

Similarly to the biotumor mixture used at IHU Strasbourg Garcia et al. (2019), an artificial lesion solution, containing muscle, agar-agar and citric acid, was prepared, strained and homogenised through needles of decreasing calibre until 18 gauge. Based on a contrast-enhanced CT image, the injection targeted location was the superior section of a medial/right liver lobe, visible through a percutaneous ultrasound (US). The solution was then percutaneously injected into the liver parenchyma, under US and fluoroscopic guidance, through a 16 gauge Secalon-T needle. Injection of 6 mL created a lesion with a diameter of approximately 20 mm. The injected artificial lesions were clearly visible in both ultrasound and CT images.

2.1.3. Placement of tracking fiducials

Based on CT and US characteristics of the artificial lesion and the surrounding vessels, for each trial, five tracking fiducials (Civco

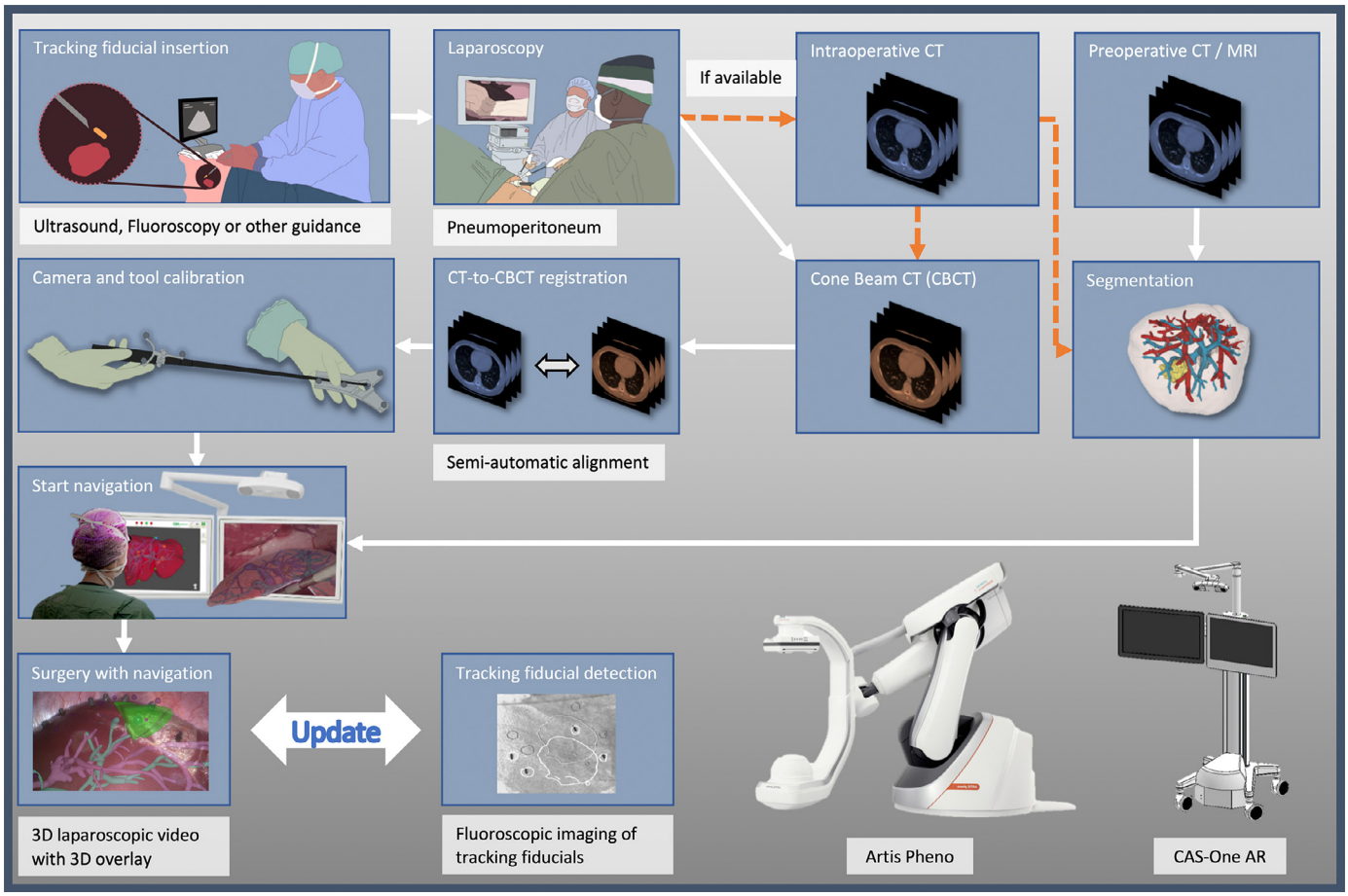

Fig. 1. Overview of the novel navigation solution with and without intraoperative CT imaging.

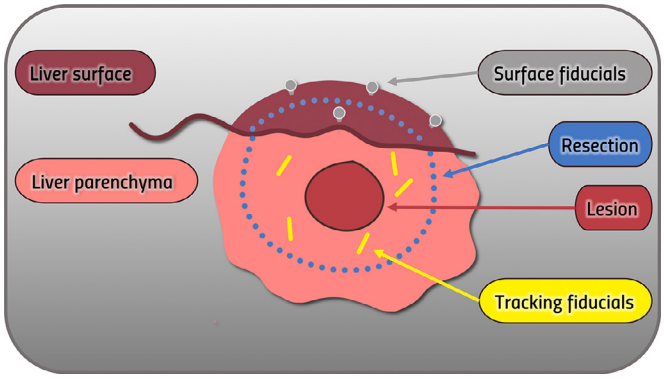

Fig. 2. Illustration to show the different fiducials: tracking fiducials were used to perform fluoroscopic updates to compensate for organ deformations, whereas surface fiducials were solely used in these trials to evaluate the accuracy of the system (and are not necessary for surgical navigation).

Radiotherapy - CyberMark 1x5mm gold rods) were aimed to be placed in the liver parenchyma within 10 mm from the lesion border (four surrounding and one underneath) (shown in Fig. 2).

2.1.4. CT And CBCT acquisition

Scans were acquired directly on the surgical table, with subjects positioned right side up in a supine position with a slight flexion. Every imaging sequence acquisition was performed with tube disconnect to have the same lung position and to lower imaging artefacts caused by breathing motion. Furthermore, Butylskopolaminbromid was given to reduce peristaltic motion. Contrast-enhanced

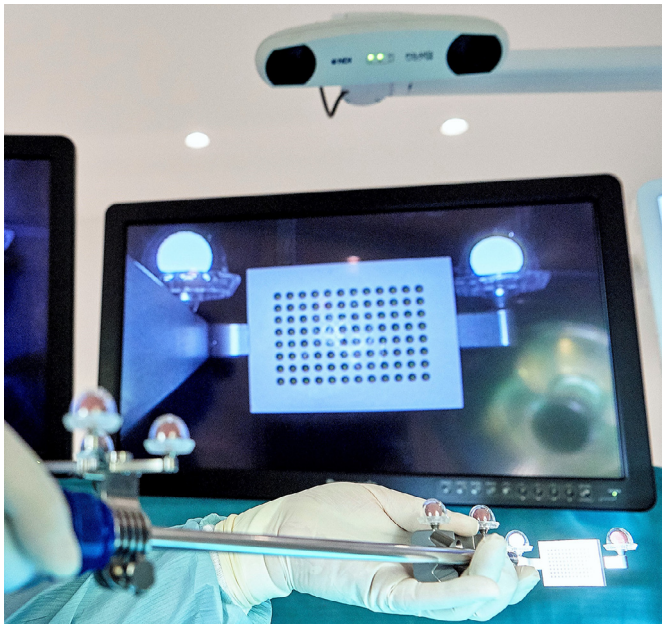

Fig. 3. Laparoscope camera calibration procedure example using the dedicated markershield.

CT images were acquired using Ombipaque 350 mg/ml via intravenous injection with 2 ml/kg for bodyweight. Injection time set for 35 seconds controlled by the flow. Portoveneous phase acquisi-

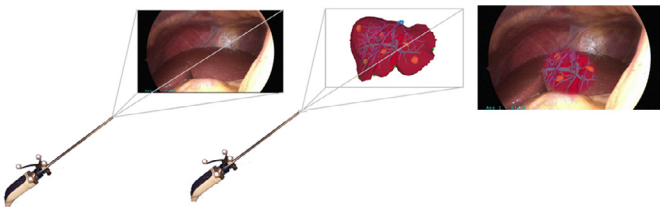

Fig. 4. Schematics explaining laparoscopic augmented reality visualization in overview mode.

tions 90 seconds after the injection start. Intraoperative CT images were acquired with pneumoperitoneum stabilized at 13 mmHg. CBCT and fluoroscopic images were acquired without contrast.

2.1.5. Segmentation

Contrast-enhanced CT images were segmented to create case-specific models by two different methods: either using a liver pre-processing method followed by semi-automatic segmentation in ITK-SNAP with manual corrections Kumar et al. (2017)·Gansawat et al. (0000) and 3D model reconstructions in 3D Slicer Fedorov et al. (2012); or using the segmentation algorithms and tools available in Syngo.via Liver Analysis. Five segmented structures were created for each case using this process: liver parenchyma, hepatic and portal vessels, a resection model and a lesion.

2.1.6. CAS-One AR Calibration

Hand-eye, camera calibration (shown in Fig. 3), and surgical instrument calibration were performed in the OR through the CAScination CAS-One system. Custom-designed optical marker shields were attached to the surgical table, instruments and calibration processes were performed as described in Prevost et al. (2019).

2.1.7. CAS-One AR Navigation

The CAS-One system provides guidance by means of an interactive 3D view of the liver model and tracked tools, as well as 3D-3D AR overlay of internal structures on the laparoscopic image. The user can choose between three different AR modes:

Overview mode: The virtual window is centred at the intersection of the laparoscope's line of sight with the liver surface. The segmented internal organ structures are rendered as seen through this virtual window shown in Fig. 4.

Region of interest mode: The virtual window is delimited by the implanted gold fiducials to limit visualization to the region of interest during the entire resection procedure.

Resection mode: The virtual window follows the tip of the tracked resection tool.

2.1.8. Registration using CT - CBCT

The solution presented in this study relies on the presence of a robotic C-arm to perform the navigation and volumetric image. In this study, CT images used for creating liver segmentations have been taken intraoperatively. However, in clinical practice, they could be a preoperative CT scan, commonly used for surgical planning, acquired typically days or weeks before the procedure. To align the CT volume and its associated segmentations to the position of the patient on the surgical table, the navigation solution requires a CBCT acquisition. An initial registration process between these two medical images is performed automatically using intensity-based 3D/3D registration algorithms available in the navigation software. This followed by manual adjustments by the surgeon (rotations and translations). In the case of liver deformations between CT and CBCT images, the rigid registration should be aimed to provide the best match in the surroundings of the lesion. The transformation matrix resulting is denoted as T_D^I according to the diagram in Fig. 5.

2.1.9. Registration using fluoroscopic updates

Laparoscopic surgery causes large motions and deformations to the shape and size of the liver Sánchez-Margallo et al. (2011) Teatini et al. (2019) Zachariadis et al. (2020) Plantefève et al. (2016). This deformation increases even further during both surgical manipulations (lifting or moving of the liver), or resection processes (liver mobilization and resections). Resection of liver parenchyma is one of the critical steps in the procedure, and most navigation solutions on the market cannot currently update the registration for the surgical navigation (Prevost et al. (2019)). The solution proposed in this study allows the user to update the surgical navigation though two fluoroscopic images were taken at different orientations with the robotic C-arm of the patient on the surgical table. To prepare the fluoroscopy-based tracking, the injected gold fiducials are automatically segmented from the CBCT volume via a threshold-based metal segmentation algorithm. The CBCT is reconstructed utilizing a metal artifact reduction algorithm, to facilitate the precise localization of the fiducials. Fiducials coordinates are determined by calculating the center of mass of the respective metal segmentation surface mesh and stored as the reference configuration. During the subsequent surgical resection, fluoroscopy images are taken along two projection angles, typically separated by at least 30 °. Through a sampling consensus algorithms, candidates of consensus sets are identified. First, the combinatorial complexity of the sampling problem is estimated based on number of detected fiducials in the two 2D fluroscopic images and number of fiducials in the CBCT. If this is below a defined threshold, deterministic sampling consensus (DETSAC) is performed, evaluating all combinatorial possibilities. However, if the number of possible combinations exceeds the runtime threshold, random sampling consensus (RANSAC) is performed instead. The resulting transformation is determined by choosing the consensus set with lowest deviations from the original 3D configuration of fiducials in the CBCT, and by prefiltering based on predefined error thresholds and boundary conditions. Based on the newly triangulated positions of the fiducials in fluoroscopy images, which reflects the movement and deformation of the liver, the navigation platform computes an additional transformation matrix T_F^P, that can update the navigation and therefore compensating organ deformations.

Positions of the tracking fiducial markers in 2D fluoroscopy images are detected using a U-Net convolutional neural network. The network was trained on various annotated images from clinical, pre-clinical and phantom settings as well as on digitally synthesized X-ray images. The robotic C-arm readily provides extrinsic and intrinsic projection matrices of image acquisition. Since all tracking fiducial markers are of the same type, a correspondence problem has to be solved in the 2D/2D/3D registration to the spatial arrangement of the fiducials in the CBCT. This is addressed by a sampling consensus algorithm. Finally, the resulting registration matrix is transferred to the navigation system which then provides up-to-date AR overlays. An example is shown in Fig. 6.

2.2. Evaluation

Evaluation of the accuracy for the navigation was conducted through two methods: TRE evaluation using additional surface

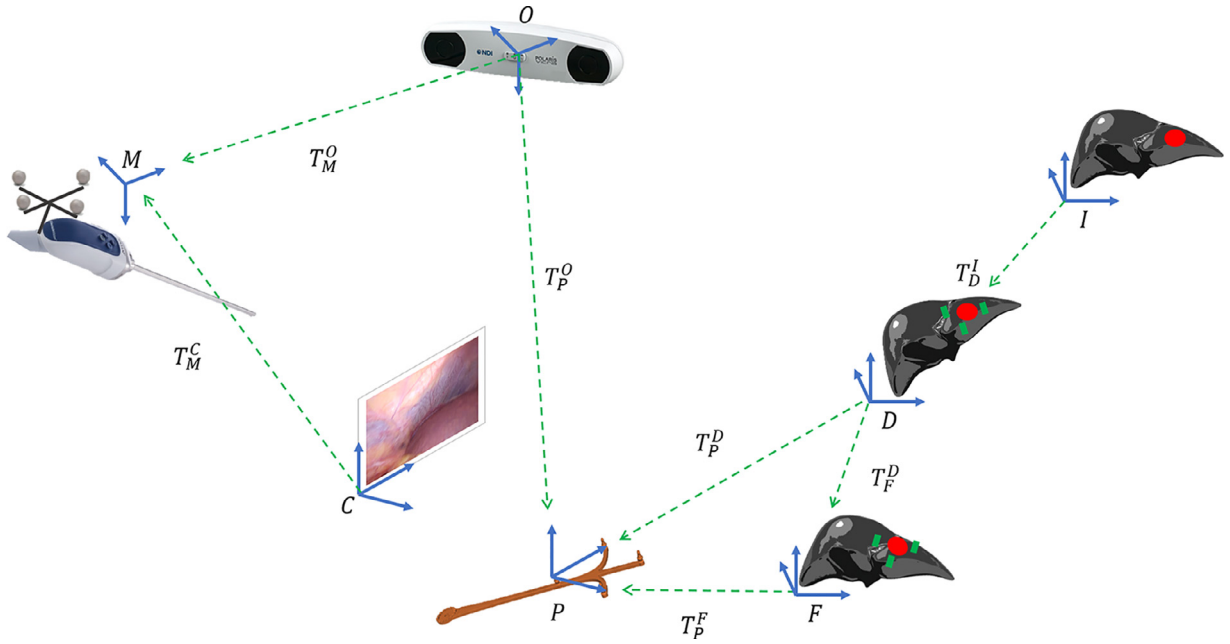

Fig. 5. Schematic of the transformation matrices involved in this surgical navigation platform. Where *O* is the coordinate system for the optical tracking system, *M* for the optical markers attached to the laparoscope camera, *C* is the coordinate system origin for the camera, *I* is the origin of the imaging modality (preoperative scan), *P* is the markerplate rigidly attached to the surgical table, *D* is the origin of the CBCT scan and *F* is the origin of the gold fiducials. The notation used in this paper indicates as superscript the coordinate system *with respects to* which the transformation is applied, and subscripted is the *towards which* coordinate system (with a row-major convention). Moreover, all transformations described in this study are 4x4 matrices in homogeneous coordinates. It is important to notice that, without using the fiducial updates, transform $(T_P^D)^{-1} = (T_P^F)^{-1} \cdot (T_F^D)^{-1}$ is the identity matrix.

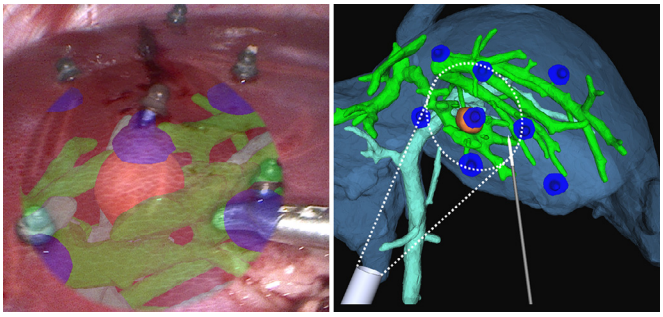

Fig. 6. Example of visualisation through navigation system monitors during laparoscopy.

Table 1
TRE fiducial evaluations averaged across the four cases (means and pooled variances in [mm], according to Altman et al. (2013)) using either the intraoperative CT scan or the fluoroscopic updates to perform the registration.

	Intraoperative CT			
	TOP	RES	DIS	ALL
Mean±SD	3.56±1.98	3.78±1.89	4.29±3.07	3.99±2.19
Number	234	797	184	1511
	Fluoroscopic Updates			
	TOP	RES	DIS	ALL
Mean±SD	3.61±1.96	4.19±2.56	7.36±5.30	5.00±3.43
Number	2868	6179	1269	10849

fiducials attached to the liver surface and computation of TRE for the resection margin marking on the liver surface. As aforementioned, both evaluation processes made use of intraoperative CT scans. These scans were used to perform segmentation of the surface fiducials and the surgical foam (which were both placed on the liver surface laparoscopically and therefore not were present in the preoperative CT scan).

2.2.1. Surface fiducials for TRE evaluation

Surface fiducials were designed and 3D printed in PA12 Smooth using a LISA Sinterit printer. These fiducials have a spherical hollow sphere with a diameter of 3.8 mm, which made them easily detectable and segmentable in the intraoperative CT. These fiducials were laparoscopically inserted on the liver surface (as shown in Fig. 2 and visible in Fig. 7), and then reprojected as AR objects on laparoscopic frames through the registration processes described in Section 2.1.8 and Section 2.1.9, an example their positions reprojected on the laparoscope camera is shown in Fig. 11. The distance between the reprojected fiducials and their physical location represents the TRE for the surgical navigation (red versus blue dots respectively in Fig. 7, similarly to Teatini et al. (2019) and Thompson et al. (2018)). Accuracy was evaluated for both AR registration approaches: using the intraoperative CT scan (Section 2.1.8), and using pairs of fluoroscopic images (Section 2.1.9). Before each fluoroscopic update, liver surgical manipulations were applied by the surgeon (to simulate the clinical scenario of wanting to update after manipulating the liver).

To describe the accuracy of the AR navigation solution, which is meant for accurate registration around the lesion (as described in Section 2), a grouping of the surface fiducials was conducted to evaluate the accuracy of AR in the regions of interest. This lead to TRE for surface fiducials to be divided into three groups (as shown in Fig. 7 and Table 2):

TOP: Liver surface fiducial inserted on top of the lesion.
RES: Liver surface fiducials within the planned resection margin (under 35 mm from the center of the lesion).
DIS: Liver surface fiducial most distal from the center of the lesion.

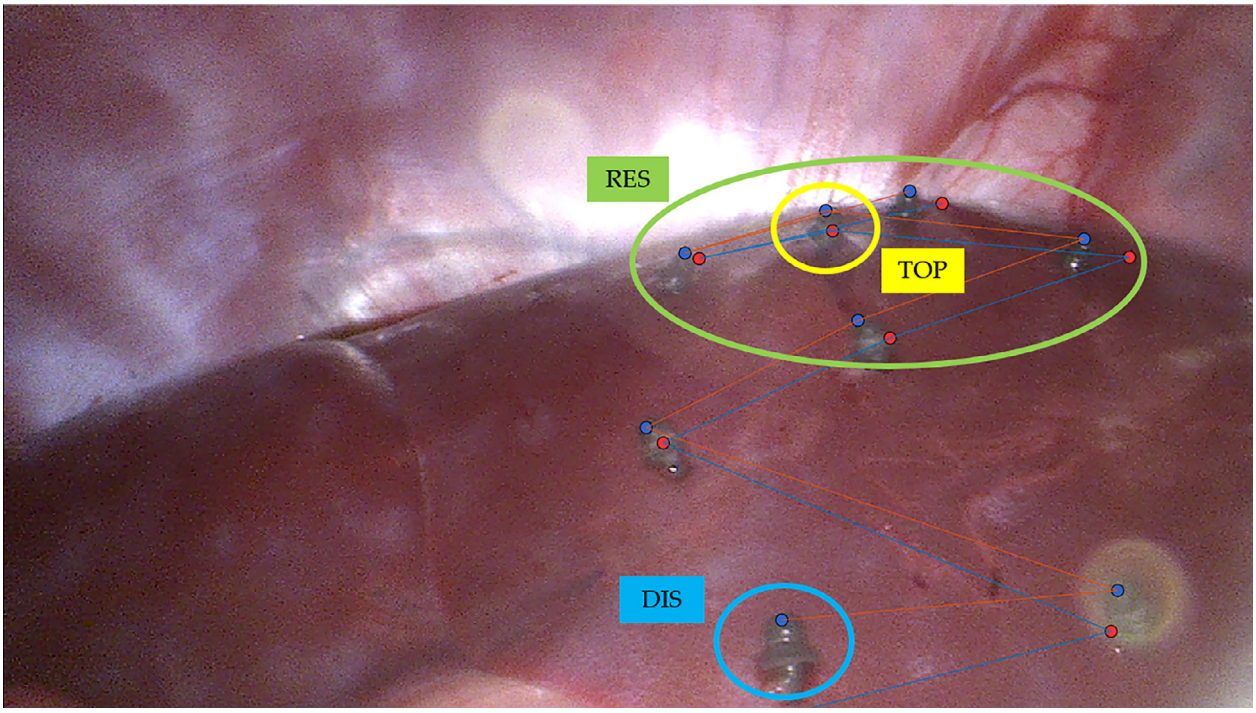

Fig. 7. Example of AR frame showing the reprojection of the liver surface fiducials. These fiducials were only used for evaluation of TRE (not necessary in clinical workflow). TRE was computed as the distance between the manually annotated positions (in blue) and the reprojected correspondent positions (in red). Furthermore, this image shows how the fiducials were classified into three groups (TOP, RES and DIS) based on their euclidean distances to the lesion. (For interpretation of the references to colour in this figure legend, the reader is referred to the web version of this article.)

Table 2
Evaluation results of TRE, in [mm] for the liver surface fiducials. The fiducials were grouped into *TOP*: the fiducial placed on top of the tumor, *RES*: fiducials within the resection margin, *DIS*: the fiducial placed furthest away from the tumor, *ALL*: all the fiducials inserted.

	Intraoperative CT															
	Case 1				Case 2				Case 3				Case 4			
	TOP	RES	DIS	ALL	TOP	RES	DIS	ALL	TOP	RES	DIS	ALL	TOP	RES	DIS	ALL
Mean	2.14	2.20	2.34	2.26	4.37	3.61	10.94	4.25	4.99	4.74	3.81	4.78	3.31	3.30	7.75	4.63
STD	1.94	1.85	1.21	1.38	1.60	1.63	1.55	2.49	1.45	1.59	1.75	1.73	0.77	1.28	0.86	2.28
Max	7.11	7.11	5.92	6.79	7.68	8.35	12.97	12.97	8.14	9.47	7.38	10.30	5.69	8.28	9.79	11.50
Num.	84	164	87	406	32	129	17	228	73	367	56	548	45	137	24	329
	Fluoroscopic Update															
	Case 1				Case 2				Case 3				Case 4			
	TOP	RES	DIS	ALL	TOP	RES	DIS	ALL	TOP	RES	DIS	ALL	TOP	RES	DIS	ALL
Mean	2.37	3.34	11.32	6.50	5.80	5.67	13.67	6.79	3.14	4.04	4.65	4.49	4.18	4.16	11.13	5.75
STD	1.09	1.59	2.26	3.46	1.83	2.53	2.29	3.45	1.46	2.57	4.33	3.28	2.90	2.41	4.49	3.36
Max	5.51	8.37	14.44	14.44	15.15	29.98	21.46	29.98	7.61	17.60	18.94	27.09	12.69	12.69	17.83	16.64
Num.	204	423	228	1068	472	720	168	1052	1960	4710	810	7964	232	326	63	765
	Comparisons intraoperative CT vs Fluoroscopic Updates															
P-value	0.21	<0.01	<0.01	<0.01	<0.01	<0.01	<0.01	<0.01	<0.01	<0.01	<0.01	0.15	0.04	0.05	<0.01	<0.01

2.2.2. Resection margin for TRE evaluation

Resection of the artificial lesion was planned on a segmented contrast-enhanced CT scan, and a separate resection volume segmentation model was created and used for the navigated resection guidance. As performed clinically, the resection margin was marked using a cauterization instrument (monopolar laparoscopic instrument) on the liver surface. Marking of the resection margin was performed following only the surgical navigation guidance, displayed as AR. To extract the spatial position of the cauterization, a surgical foam (SURGIFLO ®Hemostatic Matrix Kit) was applied on the cauterized marking on the liver. Similarly to what was performed for the liver surface fiducials, the foam was segmented from additionally acquired intraoperative CT images. The distance between the planned resection margin and the segmented foam (shown in Fig. 11) reflects the TRE of the surgical navigation, as well as the visualization inaccuracies of the AR. To quantify the error, the outline of planned resection and the segmented foam were annotated on the liver surface and then transformed into 1 mm diameter tubes using "*Markups*" and "*Markups to Models*" modules in 3D Slicer Fedorov et al. (2012) (shown in Fig. 8). A centerline was successively extracted for each tube and 50 points were sampled along the circle. Points from planned and marked resections were grouped through fuzzy-means clustering Bezdek (1981) and used to compute Hausdorff distance calculations. Distribution of these measurements is reported separately for each of the four pre-clinical cases.

2.2.3. Surgical navigation workflow evaluation

The workflow was evaluated as a measure of the time delays caused by each step in the workflow shown in Fig. 1. Time spent

Fig. 8. Example of evaluation of Target Registration Error for resection margin (Case 3). Planned resection (yellow line) and Marked resection (red line) shown on volume rendering of intraoperative CT image. (For interpretation of the references to colour in this figure legend, the reader is referred to the web version of this article.)

on intraoperative image acquisition, laparoscope and tool calibration, and navigation system setup were recorded and reported in the Section 3, as median times with min-max ranges.

2.3. Statistics description

Statistical method and statistics were chosen and completed in collaboration with statisticians at Oslo Centre for Biostatistics and Epidemiology. SPSS software (IBM Corp. Released 2017. IBM SPSS Statistics for Windows, version 25.0, Armonk, NY, USA: IBM corp) was used for the statistical analyses. Measurements in Section 3 are shown as mean with standard deviation as well as other statistical metrics in the detailed tables. Significance between TRE intraoperative CT and fluoroscopic updates were calculated using univariate ANOVAs and linear regression analysis with multiple cases and categorical variables.

3. Results

3.1. Target registration error surface fiducials

A total of 823 augmented reality frames were manually annotated across the four pre-clinical cases, for a total of 4502 manually annotated liver surface fiducials. Four intraoperative CT augmented reality evaluations were performed (one per case) whereas a total of 20 fluoroscopic updates AR evaluations were conducted (this resulted in a total of 1511 fiducials reprojected through the intraoperative CT scan-based navigation and 10849 using the fluoroscopic updates). Results averaged across the four cases, for each fiducial group, are reported in Table 1. The results for the liver surface fiducials per each case are reported in Table 2. Since unequal sample sizes were used across cases, the authors decided to make use of standard deviation pooling according to Altman et al. (2013).

Since classification into the three groups (TOP, RES, DIS) was performed based on the euclidean distances from the centre of the lesions, average distances across the four cases were 20.98 mm for TOP fiducials, 26.93 mm for RES fiducials and 69.52 mm for DIS fiducials.

To obtain exploratory results for the cases to test the hypothesis that intraoperative AR and update based AR have the same TRE, a total of 16 univariate ANOVAs (4 cases and 4 groups) were conducted comparing the TRE for each group and pre-clinical case. Results show significant differences for almost all cases, except for the TOP and RES groups (as reported in Table 2).

Table 3
Hausdorff distance in [mm] between resection plan and marked resection across 50 centerline samples per case.

	Case 1	Case 2	Case 3	Case 4
Mean	3.48	3.34	6.03	17.70
STD	1.54	0.74	2.55	8.46
Max	6.85	4.33	9.75	33.05
Q1	2.52	2.77	3.66	11.77
Q3	3.99	4.06	8.34	23.39
Q3-Q1	1.48	1.29	4.68	11.62

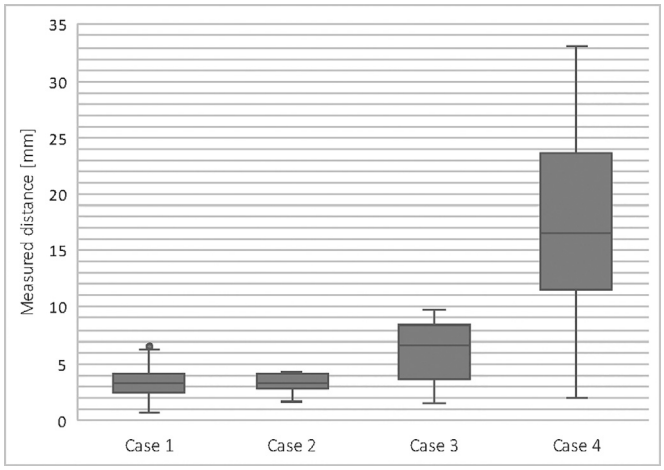

Fig. 9. Boxplot showing distribution of measured distance between planned and marked resection for each case.

3.2. Target registration error for resection margin

Measured distances between the planned and marked resection margins are listed in Table 3. Projections of both the resection plan and the marked resection on the liver surface are shown in Fig. 11. Across the four cases, based on the resection margin evaluation method, the mean median error of the surgical navigation on the liver surface was 7.47 mm, with a maximum of 33.05 mm.

Based on the results (Fig. 9), case 4 may be defined as an outlier, since the median error is more than 1.5 times the interquartile range added to the third quartile.

Fig. 10 shows an example of a resection plan and its marked resection, which follows the contour of the resection volume from the laparoscopic perspective (disregarding depth). Excluding case 4, the mean median error of the surgical navigation on the liver surface was 4.44 mm, with a maximum of 9.75 mm.

3.3. Surgical navigation workflow evaluation

Contrast-enhanced CT image acquisition median time was 13 minutes (5 - 25)(n = 18). CBCT image acquisition median time was 15 minutes (4 - 30) (n = 10). Calibration of the camera could be achieved in a median of 1:33 minutes (0:46 - 2:51) (n = 5) and 0:42 minutes (00:08 - 01:07) (n = 7) for each laparoscopic tool. Median navigation system setup time was 9:15 minutes (5:35 - 20:53) (n = 5). Median time for registration update including acquisition of two fluoroscopic images - 35 seconds (12 - 87) (n = 14).

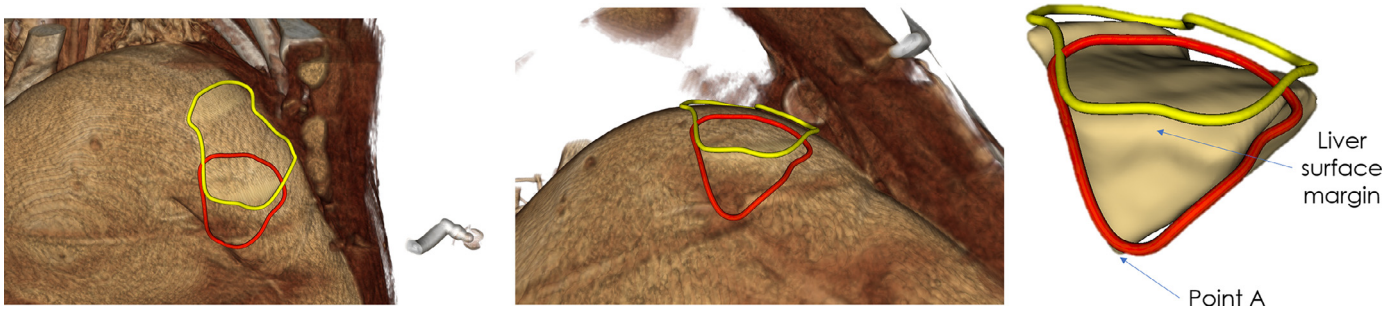

Fig. 10. Case 4. Planned resection (yellow line) and Marked resection (red line) are shown on the volume rendering of intraoperative CT image and on the planned resection. Point A was misunderstood as the projected surface resection plane, whereas it represented the depth of the resection margin underneath the lesion within the liver parenchyma. Due to this perception error, the result from Case 4 is an outlier to the rest of the cases for the margin evaluation. This error demonstrates the need to improve the AR visualization for resection margin delineation in this surgical navigation solution. (For interpretation of the references to colour in this figure legend, the reader is referred to the web version of this article.)

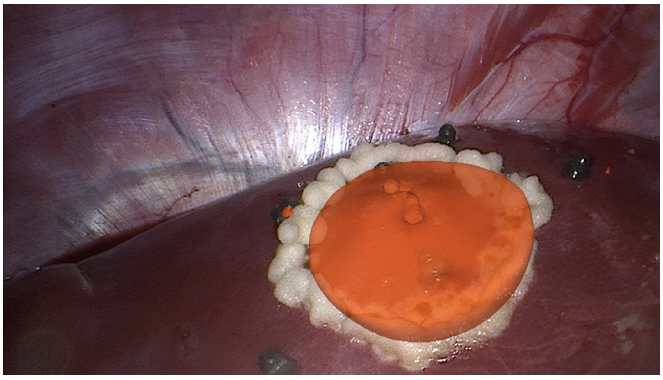

Fig. 11. Example of Augmented Reality visualization of the resection model (case 2 in this study) from the surgical navigation solution, presented in this study, together with the marked resection margin and the surgical foam used for TRE evaluation in resection margin analysis.

4. Discussion

The findings in this study show that laparoscopic navigation with satisfactory accuracy is achievable using the presented method. This novel approach, which aims to provide an accurate registration around the lesion, resulted in a very low TRE, as compared to other results available in the literature Luo et al. (2020) Thompson et al. (2018) Teatini et al. (2019) Espinel et al. (2020). Furthermore, the solution presented in this article is capable of being introduced into the clinical workflow. Moreover, since the approach presented in this article does not rely on 3D to 2D registration methods to update the registration (unlike other solutions available in the literature Espinel et al. (2020) Plantefève et al. (2016)), its accuracy is not compromised by poor laparoscopic camera visibility or bleeding, making this method one of the few methods with the capability of accurate registration during liver resection processes.

To evaluate the surgical navigation solution, surface fiducials were used to evaluate changes in TRE for the two different registration procedures available: model-to-patient registration using an intraoperative CT and fluoroscopic updates to perform registration to the CBCT. The resulting average accuracy, in terms of TRE, was 3.78±1.89 mm using intraoperative CT imaging and 4.19±2.56 mm using fluoroscopic updates after surgical manipulations were computed, which the authors believe could be accurate enough for surgical guidance.

Overall, the results in Section 3.1 and Table 2, show that AR was more accurate using the intraoperative CT scan to generate the AR (Section 2.1.8), as compared to updates (Section 2.1.9). The TRE differences, however, amounted to 0.05 mm for surgical guidance on top of the lesion and by 1.01 mm for the rest of the liver. The authors believe that this slight change in accuracy for fiducials in DIS regions may be due to lower accuracy in the triangulation of golden fiducials by using only two fluoroscopic updates (as opposed to a CT scan, which uses several projections).

The statistical analyses (Table 1) show that, for individual cases, the differences found were statistically significant. Higher accuracy closer to the lesion is expected as the method described in this study is a locally accurate registration method, which largely depends on the positions of the fiducials with respects to the lesion. For both RES and TOP fiducials, this distance was smaller than 3 cm, whereas, on average, DIS fiducials were ≈7 cm away. This increase in distance explains the decrease of accuracy further away from the position of the lesion and the tracking fiducials. However, overall, the absolute average differences between the registration methods for TOP and RES are up to ≈2 mm. For a planned liver resection with 15 mm margins, measured inaccuracies added by the updates are small enough to be used as guidance and lead to a R0 resections, which would also include tracking fiducials. Hence, this study also shows that updates may nonetheless be a valid and accurate method to continue surgical navigation in the presence of liver deformations.

To replicate one of the intended uses of the surgical navigation, marking the resection line on top of the liver, the authors conducted a further evaluation procedure for the navigation accuracy, further details in Section 3.2). This method of evaluation through resection marking incorporates additional types of inaccuracies, such as AR visualisation errors. Navigation is presented to the user in the form of an overlay of selected digital structures onto the 3D laparoscope view. The overlay, in this navigation solution, includes depth rendering for the models overlaid, although, the rendering is not fully realistic. For this reason, the surgeons claimed to need additionally/mentally fuse these overlaid resection model and the laparoscopic view of the liver. This process can create inaccuracy or misinterpretation of the presented information.

An example of this perception error caused by non-optimal visualization occurred in case 4 (Fig. 10). Evaluations using the resection marking reflect the TRE of the surface fiducials, when examining cases 1–3. Instead, case 4 resulted in an error of 17.70±8.46 mm (Table 3), as opposed to the TRE of 3.99±2.19 mm in the surface fiducial evaluation. Hence, this not an error inherent to the registration procedure. The reason for this large decrease in accuracy of the resection marking (which is an outlier to the previously examined data according to the interquartile ranges), is due to the perception error in the AR surgical navigation, as shown in Fig. 10). This error occurred during the marking of the resection because the AR reprojection of the resection was misread: the sur-

geon interpreted the bottom of the resection volume (Point A in Fig. 10) to be the proximal part of the resection. For this reason, demarcation of the resection was misaligned with respects to the planned resection margin, causing a large error estimation.

In conclusion, other than due to the statistical motivations, case 4 for the resection margin evaluation should be considered as an outlier, which can be dealt with by improving the AR visualization technique. A possible solution, for example, could be addition of a view perpendicular to the laparoscope showing tools and 3D model would present depth as horizontal different and depth perception could possibly be improved. Nevertheless, with the current visualisation solution, the navigation solution used throughout these trials could introduce errors such as that reported in case 4.

Section 2.2.3 reports timings for all the other tasks necessary for this navigation solution. Overall, on average, 26 minutes were necessary to initialize the navigation, excluding 13 minutes for the intraoperative contrast-enhanced CT imaging and 42 seconds for each laparoscopic tool to be calibrated. After the initial registration, 35 seconds on average were needed, per update, using two fluoroscopic images.

Technological achievements has led to modernization of the ORs with new intraoperative imaging technologies Mascagni et al. (2018). The use of intraoperative CBCT, associated to fluoroscopy has been proposed in the literature Oktay et al. (2013) Mountney et al. (2014). Mountney et al. combined non-rigid biomechanically driven registration between pre-operative CT and intra-operative CBCT together with stereo laparoscopic reconstruction Barillot et al. (2014), and triangulated fluoroscopic images to detect the tip of the laparoscope camera (similarly to Bernhardt et al. (2016)) to create an augmented reality system. The disadvantages of this method are that the authors attempt to register the full liver volume solely using the surface reconstruction, therefore, the method will not be able to compensate deformations during bleeding or resection steps, and, secondly, the evaluation of TRE conducted in vivo is compromised by the use of surface fiducials: since the reconstruction is used to perform the registration, any object used on the liver surface will be perfectly registered, however, this might not be true for structures within the liver tissue, such as vessels or lesions.

Nowadays, the use of hybrid registration procedures has been tested to compensate for the deformations caused by pneumoperitoneum, with surgically satisfactory accuracy although this approach requires manual interaction intraoperatively and it might prove difficult to account for deformations occurring in the back of the liver based on visual cues at the front of the liver Espinel et al. (2020), Plantefève et al. (2016), Özgür et al. (2018). Moreover, the methods described in the previously mentioned articles and other articles in the literature Soler et al. (2014); Thompson et al. (2015, 2018); Bernhardt et al. (2016), would not be able to update the registration during the steps of liver resection, which is the most critical and hazardous step in liver resection surgery.

With respects to the surgical workflow of this navigation solution, as aforementioned, this method relies on the insertion of gold fiducials around the lesion and segmentation of volumetric images such as contrast-enhanced CT. Fiducials can be inserted either percutaneously preoperatively or laparoscopically intraoperatively. The time necessary to insert the fiducials percutaneously was not examined throughout these cases, due to testing of multiple insertion techniques throughout the trials. Segmentation time was also not examined because different segmentation methods were used and tested. Moreover, segmentation time depends on quality and level of detail needed depending on image quality, anatomical complexity and extent of the region of interest.

The presented navigation method could be used with preoperative volumetric imaging, such as contrast-enhanced CT or MRI, with its respective segmentation, created beforehand and therefore not restricted by the time allocated during surgery. Registration of preoperative images from different modalities could be done automatically Wei et al. (2020). In this study, the accuracy of such approach was not evaluated, although, as mentioned before in Section 2.1.9, liver shape and intraparenchymal changes due to laparoscopy could have a significant effect on the accuracy of the navigation. This inaccuracy may be lower by using a small volume for registration such as resection with lesion and tracking fiducials compared to navigation of a larger liver region.

In clinical practise, this solution would present case-specific anatomy as a 3D model, including important structures for laparoscopic liver resection, with tracked instruments shown as well as AR overlay on laparoscopy video, similarly to the IRCAD AR navigation approach with examples shown in several clinical publications Ntourakis et al. (2016) Hallet et al. (2015). This approach can be used as an adaptable intraoperative map, which shows laparoscopic tool location in relationship to underlying anatomical structures on the 3D model or shown in the camera view. During the training of theses procedures or complex cases, this could simplify the search for specific vascular structures or the extent of the lesion in the laparoscopic US. The possibility to perform updates during an on-going resection with large deformations allows for on-demand position correction and visualisation of structures of interest with certain accuracy. This would be of great relevance for control of central point of resection bed to maintain adequate resection margins without overextending resection, outside the plan and into the healthy liver tissue. On the other hand, this additional control could also possibly reduce the rate of inadequate resection margins.

During the last decade, the definition of a successful R0 resection for CRM in the liver has been changing from 10 mm to 1 mm Postriganova et al. (2014) Hamady et al. (2014). Nevertheless, research shows that the rate of resection with resection margins below 1 mm range from 2 to 33 % Alvarez et al. (2016). Surgery guidance using the presented approach would require planning a liver resection with 15 mm margins, containing tracking fiducials within 10 mm of the lesion border. This would result in a complete resection containing both the specimen and fiducials. For cases with narrower margins, this solution provides the location of the lesion, surrounding vessels and the resection plan with reasonable accuracy, which could be controlled for with the laparoscopic US.

Enhancement to the surgical view potentially simplifies the mental burden of placing and transforming volumetric images, used for planning, to the reality in the operating room. Previous studies show a reduction of time use Pelanis et al. (2019)), reducing surgical stress Berardi et al. (2019) and cognitive load using 3D models Yeo et al. (2018)), which would allow for more focus on surgical performance. Hence, this solution could possibly allow for more advanced laparoscopic liver resections with a narrow margin close to critical structures without requiring extensive surgery times by redistributing surgical focus time. In some cases, this solution could be a resource used during the learning-curve of laparoscopic procedures to simplify some aspects of the procedure for trainees.

The navigation solution presented in this study could be used as a stepping stone towards automation of surgery by integration with robotic surgical instruments. As well as continuation of previous exploration of AR in robotic liver surgery Pessaux et al. (2015). Solution presented in this manuscript provides spatial information of intraparenchymal structures with the possibility to update during surgery without additional laparoscopic tools and could be used as a feedback system for safety mechanisms or potential automation.

The limitations of this study for TRE evaluation include: both evaluation methods were superficial and not intraparenchymal therefor navigation accuracy inside the liver was not evaluated; the ground truth positions for the surface fiducials were manual annotations conducted frame by frame and selecting the top position of the sphere of the fiducials; the foam thickness was not uniform during the application on the marked resection margin, hence, to have an equal (one point to one) comparison between the foam and the planned resection model, a 1 mm tubular structure was interpolated into the segmentation of the foam, to match the resection model margin (as shown in Fig. 11). Moreover, evaluation of the navigation accuracy using resection margin, as described in Section 3.2, was based on initial intraoperative CT registration method, without fluoroscopic updates.

The presented solution offers potential clinical benefits, however, it also introduces an additional risk of needle insertion necessary to insert the fiducial (percutaneous or laparoscopic). Overall, placement of a single gold fiducial has a documented risk of major complications in 1.1-5% and minor in 2.9–20.8% Tresch et al. (2014) Kothary et al. (2009) Kim et al. (2012) Brook et al. (2012) Hong et al. (2015) Ohta et al. (2016). For liver procedures specifically, the evidence is more limited with major 2% and minor 2-2.9% Kothary et al. (2009) Brook et al. (2012). Migration of the fiducials, which occurs for 4% of the placed fiducials, is one of the adverse events, although this does not have a documented direct association with major or minor complications Brook et al. (2012). These adverse effects reported for radiotherapy might be less pronounced in such surgical application. Fiducials are removed together with the tumour within the resectate, whereas they permanently remain in the organ in the radiotherapy use case.

Intraoperative updates of the presented navigation solution rely on fluoroscopic imaging, therefore personnel in the operating theatre require radiation protection equipment. This is not commonly needed during a typical laparoscopic liver resection at the time of writing. During this trial, operating room personnel did not detect any hinders to perform laparoscopic surgery while wearing radiation protection equipment.

Furthermore, during this trial, intraoperative CT scans were used for the navigation, which reduced the possible introduction of more inaccuracy due to registration of preoperative CT to intraoperative CBCT (CT - CBCT registration, Section 2.1.8). This inaccuracy could occur due to a more complicated registration because of the different shapes Teatini et al. (2019) Dawda et al. (2019) for the liver preoperatively and intraoperatively, after deformation caused by pneumoperitoneum.

The data reported in this study is partially based on prototype software, its future availability as a product is not guaranteed. Lastly, the studies described in this article are pre-clinical trials, and the shape and thickness of the porcine liver are different as compared to humans. The shape of the human liver is more rigid than the porcine liver, which could reduce the pneumoperitoneum deformation. In order to evaluate the effects of anatomical differences, as well as to incorporate the surgical navigation into conventional clinical workflow, clinical studies are required.

5. Conclusions

In conclusion, a novel navigation solution for liver laparoscopic surgery is presented in this study. The evaluation methods proposed show that the accuracy of the presented method could be sufficient for laparoscopic liver resection, with the possibility to perform accurate surgical navigation even in the presence of deformations or manipulations of the liver. Inclusion of the proposed navigation solution into the surgical workflow should not greatly prolong the surgery and could be useful to aid the surgeon with a 3D map of patient-specific anatomy. Additional improvements in the solution are necessary to enhance visualization methods for the navigation, especially for the AR visualization, with the possibility of displaying the resection models using different renderings approaches to avoid misinterpretation of the resection margin.

Further investigations regarding the accuracy of surgical navigation and the usability of the navigation solution should be conducted through clinical trials. Nevertheless, this solution has the potential to mitigate some of the difficulties of laparoscopic liver resection.

6. Funding

This work was supported by H2020-MSCA-ITN Marie Skodowska-Curie Actions, Innovative Training Networks (ITN) EU project number 722068 High Performance Soft Tissue Navigation (HiPerNav).

Declaration of Competing Interest

The authors declare that they have no known competing financial interests or personal relationships that could have appeared to influence the work reported in this paper.

E.P., A.T., R.P.K., O.J.E. and B.E. are co-inventors of technology licensed by the company HoloCare AS and also hold shares in the company indirectly through Inven2 AS. B.E. and T.R. are employed by Cascination AG. A.A. and A.R. are employees of Siemens Healthcare GmbH. C.R. has received research grants from Siemens Healthcare GmbH as part of a collaboration of the Technische Universitat Dresden with Siemens Healthcare GmbH.

Acknowledgements

The research leading to these results is part of the High Performance Soft-tissue Navigation (HiPerNav) project.

The authors of this study would like to express their gratitude to all the people contributed in this research. In particular, the anesthesiology, radiology and surgical staff at The Intervention Centre, Oslo University hospital - Rikshospitalet, Norway.

The authors also thank statisticians at Oslo Centre for Biostatistics and Epidemiology, at Oslo University, for statistical advisement and consultation.

References

Aghayan, D.L., Pelanis, E., smund Avdem Fretland, Kazaryan, A.M., Sahakyan, M.A., Rsok, B.I., Barkhatov, L., Bjrnbeth, B.A., Elle, O.J., Edwin, B., 2018. Laparoscopic parenchyma-sparing liver resection for colorectal metastases. Radiol. Oncol. 52 (1), 36–41.

Altman, D., Machin, D., Bryant, T., Gardner, M., 2013. Statistics with confidence: Confidence intervals and statistical guidelines. John Wiley & Sons.

Alvarez, F.A., Claria, R.S., Oggero, S., de Santibañes, E., 2016. Parenchymal-sparing liver surgery in patients with colorectal carcinoma liver metastases. World J. Gastrointest. Surg. 8 (6), 407.

Barillot, C., Hornegger, J., Howe, R., 2014. MICCAI 2014 Proceedings.

Berardi, G., Igarashi, K., Li, C.J., Ozaki, T., Mishima, K., Nakajima, K., Honda, M., Wakabayashi, G., 2019. Parenchymal sparing anatomical liver resections with full laparoscopic approach: description of technique and short-term results. Ann. Surg. XX (Xx), 1–7. doi:10.1097/SLA.0000000000003575.

Bernhardt, S., Nicolau, S.A., Agnus, V., Soler, L., Doignon, C., Marescaux, J., 2016. Automatic localization of endoscope in intraoperative CT image: a simple approach to augmented reality guidance in laparoscopic surgery. Med. Image Anal. 30, 130–143. doi:10.1016/j.media.2016.01.008.

Bernhardt, S., Nicolau, S.A., Soler, L., Doignon, C., 2017. The status of augmented reality in laparoscopic surgery as of 2016. Med. Image Anal. 37, 66–90. doi:10.1016/j.media.2017.01.007.

Bezdek, J.C., 1981. Objective Function Clustering. In: Pattern recognition with fuzzy objective function algorithms. Springer, pp. 43–93.

Brook, O.R., Gourtsoyianni, S., Mendiratta-lala, M., Siewert, B., Sheiman, R.R., Or, B., Gourtsoyianni, S., Mahadevan, A., Siewert, B., Rr, S., 2012. Biopsy in the abdomen and pelvis. February 466–470. doi:10.2214/AJR.11.6431.

Dawda, S., Camara, M., Pratt, P., Vale, J., Darzi, A., Mayer, E., 2019. Patient-specific simulation of pneumoperitoneum for laparoscopic surgical planning. J. Med. Syst. 43 (10), 317.

Espinel, Y., Özgür, E., Calvet, L., Le Roy, B., Buc, E., Bartoli, A., 2020. Combining visual cues with interactions for 3D 2D registration in liver laparoscopy. Ann. Biomed. Eng. 48 (6), 1712–1727. doi:10.1007/s10439-020-02479-z.

FDA, 2013. Indications for Use - syngo.CT Liver Analysis.

Fedorov, A., Beichel, R., Kalpathy-Cramer, J., Finet, J., Fillion-Robin, J.-C., Pujol, S., Bauer, C., Jennings, D., Fennessy, F., Sonka, M., Buatti, J., Aylward, S., Miller, J.V., Pieper, S., Kikinis, R., 2012. 3D slicer as an image computing platform for the quantitative imaging network. Magn. Reson. Imaging 30 (9), 1323–1341. doi:10.1016/j.mri.2012.05.001.

Fretland, A., Dagenborg, V.J., Waaler Bjørnelv, G.M., Aghayan, D.L., Kazaryan, A.M., Barkhatov, L., Kristiansen, R., Fagerland, M.W., Edwin, B., Andersen, M.H., 2019. Quality of life from a randomized trial of laparoscopic or open liver resection for colorectal liver metastases. British Journal of Surgery 106 (10), 1372–1380. doi:10.1002/bjs.11227.

Gansawat, D., Jirattiticharoen, W., Sotthivirat, S., Koonsanit, K., Narkbuakaew, W., Yampri, P., Sinthupinyo, W.,. Integration of Image Processing from the Insight Toolkit (ITK) and the Visualization Toolkit (VTK) in Java Language for Medical Imaging Applications. In: IFMBE Proceedings. Springer Berlin Heidelberg, pp. 586–589. doi:10.1007/978-3-540-92841-6_144.

Garcia, A., Lastname, N., et al, 2019. Simulation and Navigation surgery for LLR (NEEDS FIX).

Hallet, J., Soler, L., Diana, M., Mutter, D., Baumert, T.F., Habersetzer, F., Marescaux, J., Pessaux, P., 2015. Trans-thoracic minimally invasive liver resection guided by augmented reality. J. Am. Coll. Surg. 220 (5), e55–e60. doi:10.1016/j.jamcollsurg.2014.12.053.

Hamady, Z.Z.R., Lodge, J.P.A., Welsh, F.K., Toogood, G.J., White, A., John, T., Rees, M., 2014. One-Millimeter cancer-Free margin is curative for colorectal liver metastases: A Propensity score case-Match approach. Ann. Surg. 259 (3).

Hilal, M.A., Aldrighetti, L., Dagher, I., Edwin, B., Troisi, R.I., Alikhanov, R., Aroori, S., Belli, G., Besselink, M., Briceno, J., Gayet, B., D'Hondt, M., Lesurtel, M., Menon, K., Lodge, P., Rotellar, F., Santoyo, J., Scatton, O., Soubrane, O., Sutcliffe, R., Van Dam, R., White, S., Halls, M.C., Cipriani, F., Van Der Poel, M., Ciria, R., Barkhatov, L., Gomez-Luque, Y., Ocana-Garcia, S., Cook, A., Buell, J., Clavien, P.A., Dervenis, C., Fusai, G., Geller, D., Lang, H., Primrose, J., Taylor, M., Van Gulik, T., Wakabayashi, G., Asbun, H., Cherqui, D., 2018. The southampton consensus guidelines for laparoscopic liver surgery: from indication to implementation. Ann. Surg. 268 (1), 11–18. doi:10.1097/SLA.0000000000002524.

Hong, T.S., Nm, K., Ts, H., Kambadakone, A., 2015. Proton Beam Therapy of Liver Rate and Complications (February),207–213. 10.2214/AJR.14.12901

Kim, J.H., Hong, S.S., Kim, J.H., Park, H.J., Chang, Y.-w., Chang, A.R., Kwon, S.-b., 2012. Safety and efficacy of ultrasound-Guided fiducial marker implantation for cyberknife radiation therapy 13 (3), 307–313.

Kothary, N., Heit, J.J., Louie, J.D., Kuo, W.T., Loo, B.W., Koong, A., Chang, D.T., Hovsepian, D., Sze, D.Y., Hofmann, L.V., 2009. Safety and efficacy of percutaneous fiducial marker implantation for image-guided radiation therapy. Journal of Vascular and Interventional Radiology 20 (2), 235–239. doi:10.1016/j.jvir.2008.09.026.

Kumar, R.P., Barkhatov, L., Edwin, B., Albregtsen, F., Elle, O.J., 2017. Portal and Hepatic Vein Segmentation with Leak Restriction: A Pilot Study. In: EMBEC & NBC 2017. Springer Singapore, pp. 823–826. doi:10.1007/978-981-10-5122-7_206.

Luo, H., Yin, D., Zhang, S., Xiao, D., He, B., Meng, F., Zhang, Y., Cai, W., He, S., Zhang, W., Hu, Q., Guo, H., Liang, S., Zhou, S., Liu, S., Sun, L., Guo, X., Fang, C., Liu, L., Jia, F., 2020. Augmented reality navigation for liver resection with a stereoscopic laparoscope. Computer Methods and Programs in Biomedicine 187, 105099. doi:10.1016/j.cmpb.2019.105099.

Mascagni, P., Longo, F., Barberio, M., Seeliger, B., Agnus, V., Saccomandi, P., Hostettler, A., Marescaux, J., Diana, M., 2018. New intraoperative imaging technologies: innovating the surgeon's eye toward surgical precision. J. Surg. Oncol. 118 (2), 265–282. doi:10.1002/jso.25148.

Modrzejewski, R., Collins, T., Seeliger, B., Bartoli, A., Hostettler, A., Marescaux, J., 2019. An in vivo porcine dataset and evaluation methodology to measure soft-body laparoscopic liver registration accuracy with an extended algorithm that handles collisions. Int. J. Comput. Assist. Radiol. Surg. 14 (7), 1237–1245.

Mountney, P., Fallert, J., Nicolau, S., Soler, L., Mewes, P.W., 2014. An augmented reality framework for soft tissue surgery. In: International Conference on Medical Image Computing and Computer-Assisted Intervention. Springer, pp. 423–431.

Nicolau, S.A., Pennec, X., Soler, L., Buy, X., Gangi, A., Ayache, N., Marescaux, J., 2009. An augmented reality system for liver thermal ablation: design and evaluation on clinical cases. Med. Image Anal. 13 (3), 494–506. doi:10.1016/j.media.2009.02.003.

Ntourakis, D., Memeo, R., Soler, L., Marescaux, J., Mutter, D., Pessaux, P., 2016. Augmented reality guidance for the resection of missing colorectal liver metastases: an initial experience. World J. Surg. 40 (2), 419–426. doi:10.1007/s00268-015-3229-8.

Ohta, K., Shimohira, M., Murai, T., Nishimura, J., Iwata, H., Ogino, H., Hashizume, T., Shibamoto, Y., 2016. Percutaneous fi ducial marker placement prior to stereotactic body radiotherapy for malignant liver tumors : an initial experience 57 (2), 174–177. doi:10.1093/jrr/rrv099.

Oktay, O., Zhang, L., Mansi, T., Mountney, P., Mewes, P., Nicolau, S., Soler, L., Chefd hotel, C., 2013. Biomechanically driven registration of pre-to intra-operative 3d images for laparoscopic surgery. In: International Conference on Medical Image Computing and Computer-Assisted Intervention. Springer, pp. 1–9.

Özgür, E., Koo, B., Le Roy, B., Buc, E., Bartoli, A., 2018. Preoperative liver registration for augmented monocular laparoscopy using backward forward biomechanical simulation. Int. J. Comput. Assist. Radiol. Surg. 13 (10), 1629–1640. doi:10.1007/s11548-018-1842-3.

Palomar, R., Cheikh, F.A., Edwin, B., Fretland, Å., Beghdadi, A., Elle, O.J., 2017. A novel method for planning liver resections using deformable bézier surfaces and distance maps. Comput. Methods Programs Biomed. 144, 135–145. doi:10.1016/j.cmpb.2017.03.019.

Pelanis, E., Kumar, R.P., Aghayan, D.L., Palomar, R., Fretland, Å.A., Brun, H., Elle, O.J., Edwin, B., 2019. Use of mixed reality for improved spatial understanding of liver anatomy. Minimally Invasive Therapy & Allied Technologies 1–7. doi:10.1080/13645706.2019.1616558.

Pessaux, P., Diana, M., Soler, L., Piardi, T., Mutter, D., Marescaux, J., 2015. Towards cybernetic surgery: robotic and augmented reality-assisted liver segmentectomy. Langenbeck's Archives of Surgery 400 (3), 381–385. doi:10.1007/s00423-014-1256-9.

Plantefève, R., Peterlik, I., Haouchine, N., Cotin, S., 2016. Patient-specific biomechanical modeling for guidance during minimally-invasive hepatic surgery. Ann. Biomed. Eng. 44 (1), 139–153.

Postriganova, N., Kazaryan, A.M., Røsok, B.I., Fretland, Å.A., Barkhatov, L., Edwin, B., 2014. Margin status after laparoscopic resection of colorectal liver metastases : does a narrow resection margin have an influence on survival and local recurrence ?, 822–829, doi:10.1111/hpb.12204.

Prevost, G.A., Eigl, B., Paolucci, I., Rudolph, T., Peterhans, M., Weber, S., Beldi, G., Candinas, D., Lachenmayer, A., 2019. Efficiency, accuracy and clinical applicability of a new image-guided surgery system in 3d laparoscopic liver surgery. Journal of Gastrointestinal Surgery 1–8.

Quero, G., Lapergola, A., Soler, L., Marescaux, J., Mutter, D., Pessaux, P., 2019. Virtual and augmented reality in oncologic liver surgery. Surg. Oncol. Clin. N. Am. 28 (1), 31–44. doi:10.1016/j.soc.2018.08.002.

Sánchez-Margallo, F.M., Moyano-Cuevas, J.L., Latorre, R., Maestre, J., Correa, L., Pagador, J.B., Sánchez-Peralta, L.F., Sánchez-Margallo, J.A., Usón-Gargallo, J., 2011. Anatomical changes due to pneumoperitoneum analyzed by MRI: an experimental study in pigs. Surgical and Radiologic Anatomy 33 (5), 389–396. doi:10.1007/s00276-010-0763-9.

Soler, L., Mutter, D., Pessaux, P., Marescaux, J., 2015. Patient specific anatomy: the new area of anatomy based on computer science illustrated on liver.. J. Visc. Surg. 1 (8), 21. doi:10.3978/j.issn.2221-2965.2015.11.06.

Soler, L., Nicolau, S., Pessaux, P., Mutter, D., Marescaux, J., 2014. Real-time 3d image reconstruction guidance in liver resection surgery. Hepatobiliary. Surg. Nutr. 3 (2), 73.

Teatini, A., de Frutos, J.P., Eigl, B., Pelanis, E., Aghayan, D.L., Lai, M., Kumar, R.P., Palomar, R., Edwin, B., Elle, O.J., 2020. Influence of sampling accuracy on augmented reality for laparoscopic image guided surgery.. Minimally Invasive Therapy & Allied Technologies 1–7. doi:10.1080/13645706.2020.1727524.

Teatini, A., Langø, T., Edwin, B., Elle, O., et al., 2018. Assessment and comparison of target registration accuracy in surgical instrument tracking technologies. In: 2018 40th Annual International Conference of the IEEE Engineering in Medicine and Biology Society (EMBC). IEEE, pp. 1845–1848.

Teatini, A., Pelanis, E., Aghayan, D.L., Kumar, R.P., Palomar, R., Fretland, Å.A., Edwin, B., Elle, O.J., 2019. The effect of intraoperative imaging on surgical navigation for laparoscopic liver resection surgery. Sci. Rep. 9 (1), 1–11.

Teber, D., Guven, S., Simpfendörfer, T., Baumhauer, M., Güven, E.O., Yencilek, F., Gözen, A.S., Rassweiler, J., 2009. Augmented reality: a new tool to improve surgical accuracy during laparoscopic partial nephrectomy? preliminary in vitro and in vivo results. Eur. Urol. 56 (2), 332–338.

Thompson, S., Schneider, C., Bosi, M., Gurusamy, K., Ourselin, S., Davidson, B., Hawkes, D., Clarkson, M.J., 2018. In vivo estimation of target registration errors during augmented reality laparoscopic surgery. Int. J. Comput. Assist. Radiol. Surg. 13 (6), 865–874.

Thompson, S., Totz, J., Song, Y., Johnsen, S., Stoyanov, D., Ourselin, S., Gurusamy, K., Schneider, C., Davidson, B., Hawkes, D., Clarkson, M.J., 2015. Accuracy validation of an image guided laparoscopy system for liver resection. In: Webster, R.J., Yaniv, Z.R. (Eds.), Medical Imaging 2015: Image-Guided Procedures, Robotic Interventions, and Modeling. SPIE doi:10.1117/12.2080974.

Tresch, E., Jarraya, H., Bonodeau, F., Lacornerie, T., Mirabel, X., Boulanger, T., Taieb, S., Kramar, A., Lartigau, E., Ceugnart, L., 2014. Novel Technique for Hepatic Fiducial Marker Placement for Stereotactic Body Radiation Therapy. doi:10.1016/j.ijrobp.2014.05.002.

Wei, D., Ahmad, S., Huo, J., Huang, P., Yap, P.T., Xue, Z., Sun, J., Li, W., Shen, D., Wang, Q., 2020. SLIR: Synthesis, localization, inpainting, and registration for image-guided thermal ablation of liver tumors. Med. Image Anal. 65, 101763. doi:10.1016/j.media.2020.101763.

Yeo, C.T., MacDonald, A., Ungi, T., Lasso, A., Jalink, D., Zevin, B., Fichtinger, G., Nanji, S., 2018. Utility of 3D reconstruction of 2D liver computed tomography/magnetic resonance images as a surgical planning tool for residents in liver resection surgery. J. Surg. Educ. 75 (3), 792–797. doi:10.1016/j.jsurg.2017.07.031.

Zachariadis, O., Teatini, A., Satpute, N., Gómez-Luna, J., Mutlu, O., Elle, O.J., Olivares, J., 2020. Accelerating b-spline interpolation on gpus: application to medical image registration. Comput. Methods Programs Biomed. 105431.